Advances in Geo-Energy Research

Vol. 22, No. 2, p. 103-117, 2026

Original article

Occurrence states of organic matter modulate the surface properties of shale nanopores

Xu Li[1,2], Jingong Cai[2], Huimin Liu[3], Junliang Li[3], Zheng Li[3], Jianchao Cai[4]*

[1]*College of Geophysics and Petroleum Resources, Yangtze University, Wuhan 430100, P. R. China*

[2]*State Key Laboratory of Marine Geology, Tongji University, Shanghai 200092, P. R. China*

[3]*Exploration and Development Research Institute of Shengli Oilfield Company, SINOPEC, Dongying 257015, P. R. China*

[4]*State Key Laboratory of Petroleum Resources and Engineering, China University of Petroleum, Beijing 102249, P. R. China*

Keywords:
Wettability
surface potential
organic matter occurrence states
shale nanopores
fluid invasion

Cited as:
Li, X., Cai, J., Liu, H., Li, J., Li, Z., Cai, J. Occurrence states of organic matter modulate the surface properties of shale nanopores. Advances in Geo-Energy Research, 2026, 22(2): 103-117. https://doi.org/10.46690/ager.2026.11.02

Abstract:
The surface properties of shale nanopores, governed by the coexistence of mineral surfaces and adsorbed organic matter, fundamentally controls fluid invasion, occurrence, and mobility in confined spaces and is therefore critical for shale oil and gas recovery. However, the individual contributions of organic matter with different occurrence states to wettability and surface potential remain poorly quantified. In this work, these contributions were decoupled using successive dichloromethane extraction and sodium hypochlorite oxidation, combined with multiple geochemical and petrophysical characterization methods. Experimental results confirmed progressive organic matter removal and the liberation of pore wall surfaces. The removal of solvent-extractable organic matter reduces the water contact angle, while that of organic matter through subsequent oxidation causes further reduction. Surface potential measurements also revealed that the removal of organic matter with different occurrence states exerts distinct effects on the electrochemical properties of pore walls. Work of adhesion calculations indicated an increasing trend during progressive organic matter removal, quantitatively linking organic matter occurrence to interfacial free energy. The observed fluid imbibition behavior demonstrated that invasion into sub-100 nm pores is selectively hindered by residual organic matter, and the second-stage imbibition rate correlates positively with wettability. These findings establish a quantitative link between organic matter adsorption states and nanoscale interfacial properties, they providing a mechanistic framework for predicting fluid behavior in organic rich shales and offering theoretical support for understanding shale wettability alteration and optimizing surfactant selection.

1. Introduction

Shales contain abundant nanoscale pores, and the occurrence and flow behavior of fluids therein control the oil-bearing property and mobility of shale oil and gas. These processes are crucial for the efficient exploration and development of shale oil and gas resources. The occurrence and flow of fluids in nanopores are strongly controlled by the nature of pore wall-fluid interfacial interactions (Dong et al., 2019; Cui et al., 2025). Wettability and electrical properties obtained from contact angle and surface potential measurements are important means for evaluating the characteristics of pore wall-fluid interfacial interactions and predicting fluid flow behavior (Isah et al., 2022; Cai et al., 2024). The controlling factors of shale wettability have been widely investigated, regarding the effects of mineral composition, temperature, pressure, ionic strength, etc. (Jia et al., 2025; Zheng et al., 2025). Moreover, a

Yandy Scientific Press

*Corresponding author.
E-mail address: a18765922983@163.com (X. Li); jgcai@tongji.edu.cn (J. Cai); hmliu@vip.163.com (H. Liu); lijunliang.slyt@sinopec.com (J. Li); Lizheng761.slyt@sinopec.com (Z. Li); caijc@cup.edu.cn (J. Cai).
2207-9963 © The Author(s) 2026.
Received August 26, 2026; revised September 27, 2026; accepted October 13, 2026; available online October 16, 2026.

positive correlation has been reported between organic matter abundance and rock-air-water contact angle (Singh et al., 2016; Begum et al., 2019). The authors also noted that organic matter occurrence significantly modifies the adsorption behavior (Kholodov et al., 2018; Shah et al., 2018) and electrochemical properties (Huang et al., 2026) of minerals. Nevertheless, the role of organic matter occurrence remains poorly constrained, particularly across different occurrence states.

Wettability is a key quantitative parameter characterizing fluid-solid interfacial interactions. Shale wettability is strongly heterogeneous and arises from internal and external factors. The latter, encompassing fluid chemistry, temperature and pressure, have been relatively well studied (Li et al., 2025; Xia et al., 2026). Internal factors include the complex mineral and organic matter compositions of shale; different minerals (Zhang et al., 2025; Wang et al., 2026b) as well as kerogen of different types and maturities (Suekuni et al., 2024; Fu et al., 2025) can produce contrasting wetting behaviors. Variable wettability leads to significant differences in the spatial distribution, occurrence mode (adsorbed-to-free ratio) and flow behavior of fluids in pores (Jiao et al., 2024; Cai et al., 2026). Pore walls with different attributes have distinct properties. Combined with the proportions of different pore-wall types (Iltaf et al., 2025; Sun et al., 2026) and changes in pore wall types during diagenetic transformation (Wang et al., 2024; Chen et al., 2025), the wettability of shales with different compositions and at different evolutionary stages can be predicted. However, while external fluid and environmental factors have been emphasized (Jia et al., 2025), existing research on internal factors is mainly simulation-based and lacks macroscopic systematic studies. Attention to organic matter has also been limited to comparisons between kerogen and minerals or among kerogens of different types and maturities (Begum et al., 2019; Lawal et al., 2020). However, organic matter in shale exists not only in the form of kerogen but also soluble organic matter and mineral bounded organic matter (Cai et al., 2020). To this end, the distinct contributions of organic matter in different states to wettability remain poorly understood.

The characterization of electrochemical properties is likewise an integral component in the study of the modes and mechanisms of solid-fluid interactions (Koopal, 2012; Zhang et al., 2026). These properties govern the binding modes and strengths between molecules of different chemical activities in fluids and minerals or mineral-organic composites (Kleber et al., 2021). Surfactant flooding is a widely employed enhanced oil recovery (EOR) method. Surfactants are classified by headgroup charge into cationic, anionic and nonionic types (Isah et al., 2022). The selection of an appropriate surfactant type depends on the specific reservoir characteristics (Pal et al., 2018). The conventional principle for surfactant selection is that cationic surfactants are matched to negatively charged surfaces. However, the occurrence of organic matter on pore-wall surfaces can mask the charge properties of the underlying minerals and alter both the polarity and electrochemical activity of the pore wall surface (Chorover et al., 2004). If surfactants are selected solely based on electrokinetic detection results, the selection may fail, thereby reducing EOR efficiency. Therefore, how organic matter affects the electrochemical properties of minerals also warrants attention.

More importantly, organic matter in shale does not exist in isolation but forms mineral-organic complexes with minerals through physical and chemical interactions such as hydrogen bonding, hydrophobic interactions, cation exchange, and cation bridging (Kleber et al., 2021; Zhang et al., 2025). Different binding modes imply different binding strengths, providing a possibility for separating organic matter with different occurrence states. The commonly used separation methods include solvent extraction (Zhang et al., 2025), chemical wet oxidation (Mikutta et al., 2005), and thermal treatment (Mayer et al., 2004; Wagai et al., 2009). However, residual samples from the thermal treatment method often suffer from structural damage due to dehydration (Kok et al., 2023; Sun et al., 2026), making them unsuitable for wettability characterization. In contrast, solvent extraction only removes soluble organic matter and does not damage minerals. Similarly, the sodium hypochlorite (NaClO) oxidation method has been proven to cause weak mineral damage (Siregar et al., 2005; Li et al., 2020). Therefore, it is favorable to combine solvent extraction with dichloromethane (CH_2Cl_2) and oxidation by NaOCl for sample pretreatment to remove organic matter occurring in different states (Zhu et al., 2016). The novelty of the present study lies in combining successive separation with contact angle and surface potential measurements to quantify the distinct contributions of organic matter occurrence states to pore wall interfacial properties and fluid flow. Atomic force microscopy (AFM) provides high-resolution surface topography and, in Kelvin probe modes, the quantitative mapping of nanoscale surface potential (Yin et al., 2012; Walker et al., 2017). This enables a direct assessment of the electrical heterogeneity of pore walls before and after organic matter removal. Imbibition, driven by capillary and interfacial forces, is a sensitive probe of pore wall-fluid interactions: The imbibition rate and imbibed volume reflect the dynamic behavior of confined fluids (Lv et al., 2025; Zheng et al., 2025). Combining these two methods with contact angle detection allows linking molecular-scale interfacial properties to macroscopic fluid invasion behavior.

In this study, a successive treatment method was used to separate organic matter in different occurrence states. To characterize the wettability and surface potential of samples, contact angle and AFM measurements were performed before and after treatment, revealing the controlling effect of organic matter occurrence states on the interfacial properties. Samples with different lithofacies were selected for spontaneous imbibition to investigate the relationship between wettability and fluid flow, in order to identify differences in wetting behavior and their controlling effect on the imbibition process. We also aimed to clarify the importance of interfacial properties research in pore wall-fluid interaction studies. The findings have important theoretical and practical value for shale oil resource evaluation and the optimization of EOR methods.

2. Materials and methods

2.1 Materials and pretreatments

Argillaceous source rock samples were collected from the Dongying Sag, Bohai Bay Basin, China, covering depths of 3,300-4,330 m within the Shahejie Formation (Table S1). They were crushed to 20 mesh and divided into three groups: (1) untreated raw samples; (2) samples subjected to Soxhlet extraction using a 9:1 dichloromethane/methanol mixture at 48 ± 2 °C for 10 days (Mikutta et al., 2005); and (3) samples extracted and further oxidized using a 6% NaClO solution (pH 8) at room temperature (Li et al., 2020). Since reduced reaction times and fewer cycles have been shown to decrease organic matter removal efficiency (Kaiser and Guggenberger, 2003; Siregar et al., 2005), 8 cycles, each with a 12-hour reaction time, were implemented to ensure more complete organic matter removal. After oxidation, samples were soaked in deionized water for about 30 minutes, rinsed three times to remove residual salts and oxidant, and dried for analysis and testing. Because contact angle results are strongly affected by surface roughness, samples in all three of groups were ground to 200 mesh and pressed using an HY-12 press at 30 MPa for 200 s. The effectiveness of the pressing conditions was verified by AFM height measurements. Samples with different lithofacies were selected for surface potential detection. The core columns (2.5 cm in diameter) of Samples 27, 28, 31, and 34 (differing in lithofacies and organic matter content) were drilled parallel to the bedding plane via wireline cutting for imbibition and nuclear magnetic resonance (NMR) tests. All samples before and after pretreatments underwent Rock-Eval pyrolysis, as well as N_2 adsorption and contact angle detections to obtain the total organic carbon (TOC), S_1, S_2, specific surface area (SSA), and contact angle values (Tables S1 and S2; Fig. 1).

2.2 Pyrolysis

Pyrolysis was performed on a Rock-Eval VI instrument following the Chinese National Standard GB/T 18602-2001. After grinding to 200 mesh, samples were heated under helium flow. Hydrocarbons were detected using a hydrogen flame ionization detector, while CO_2 was measured with a thermal conductivity detector. The instrument was preheated to a constant temperature of 300 °C, after which approximately 60-70 mg of each sample was introduced. Initially, the samples were kept at 300 °C for 3 min to obtain free hydrocarbons S_1. Then, the temperature was raised to 600 °C at 25 °C/min to obtain cracking hydrocarbons (S_2) and CO/CO_2 generated during the pyrolysis reaction (S_3CO, S_3). Finally, the samples were cooled to 300 °C, transferred to an oxidation furnace, and heated to 850 °C at a rate of 25 °C/min to quantify CO/CO_2 generated from the oxidation reaction (S_4CO, S_4). A blank and a duplicate were included for every ten samples. TOC content was calculated based on the measured parameters according to GB/T 18602-2001.

2.3 SSA

Approximately 1-2 g of sample was crushed to a particle size of 20 mesh and degassed by keeping at 80 °C for more than 6 hours under vacuum (10 μm Hg) to remove adsorbed moisture and volatile matter prior to the low-temperature (77 K) N_2 adsorption analysis. Measurements in the adsorption mode were performed over the relative pressure (P/P_0) range of 0.001-0.995. Then, the SSA for each sample was determined by the inversion of adsorption branch of the isotherm using the Brunauer-Emmett-Teller analysis procedure at a relative pressure range of 0.05-0.30 (Brunauer et al., 1938). The molecular sectional area of N_2 was 0.162 nm^2.

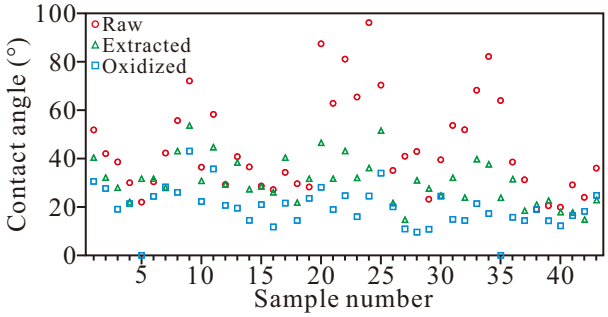


Fig. 1. Contact angles before and after pretreatments for each sample.

2.4 Interfacial characteristics

2.4.1 AFM and Kelvin probe force microscopy

Gold-coated silicon probes (Au-coated Si) were used for both the topographic and Kelvin probe force microscopy (KPFM) measurements. All measurements were performed in air under ambient conditions (room temperature, 40% relative humidity). Topographic images were acquired in semi-contact (intermittent-contact) mode at a resolution of 512 × 512 pixels, with a scan rate of 1 Hz. KPFM was performed simultaneously with topography using a two-pass amplitude-modulation scheme. In the first pass, the surface morphology was recorded in semi-contact mode; in the second pass, the Au-coated silicon probe retraced the surface potential profile at a constant lift height of 100 nm above the surface.

2.4.2 Contact angle

The contact angle of samples before and after sequential processing was measured using the sessile drop method with 4 μL deionized water droplets at 20-25 °C and 40%-60% relative humidity. Due to its effectiveness in describing droplet interfacial behavior, the Young-Laplace equation was applied for fitting the droplet profiles to determine the contact angles.

2.5 Spontaneous imbibition

Samples were first dried in an oven at 60 °C until a constant weight was achieved, then their initial mass was recorded. During imbibition, each sample was placed vertically on a permeable stone, and the mass was measured to quantify water uptake (Table S3). NMR measurements were simultaneously performed to monitor fluid distribution and pore structure evolution throughout the process (magnetic field strength: 0.3 ± 0.05 T. resonance frequency: 12 MHz). The Carr-Purcell-Meiboom-Gill sequence was employed to acquire the T_2 relaxation time spectra under the following parameters: A waiting time of 4,000 ms, an echo spacing of 0.15 ms, a total

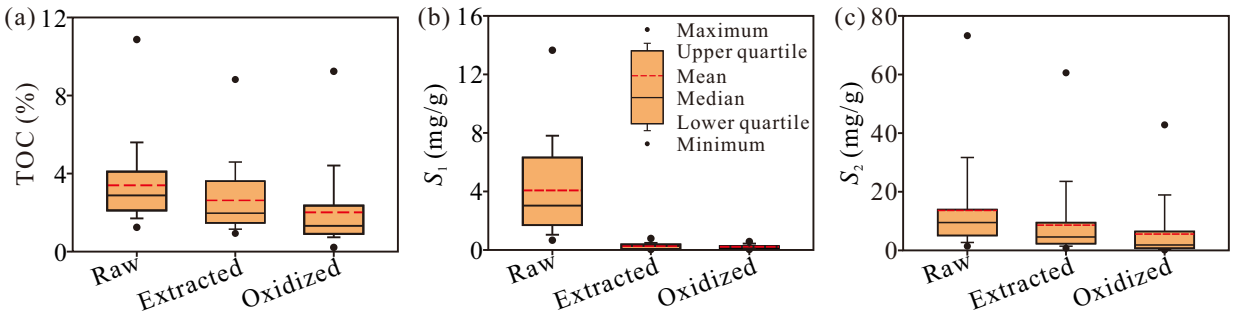


Fig. 2. Comparisons of the (a) TOC, (b) S_1 and (c) S_2 of raw, extracted and oxidized samples.

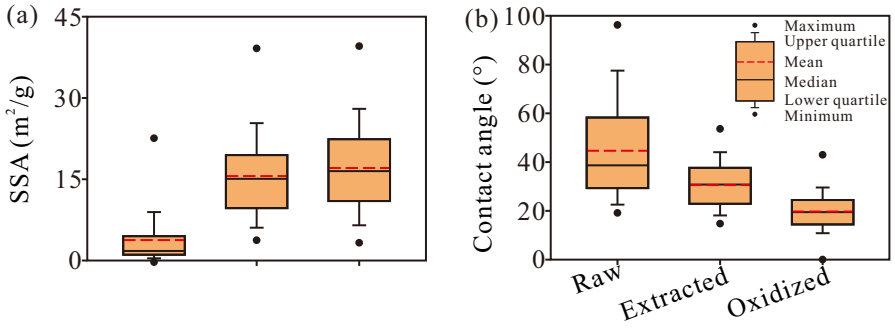


Fig. 3. Changes in (a) SSA and (b) contact angle in response to pretreatments.

of 12,000 echoes and 32 scans, and a controlled temperature of 25 °C.

2.6 X-ray diffraction

Bulk mineral composition was detected by X-ray diffraction on samples used for the AFM and imbibition tests to better explain the causes of differences in their imbibition and surface potential characteristics. The testing procedure was carried out in accordance with the petroleum and natural gas industry standard SY/T 6210-1996. The specific conditions were: A Cu target with a tube voltage of 30 kV and a tube current of 40 mA. The scan rate was set at 2° (2θ) per minute, covering a 2θ range of 3° to 40°.

3. Results

3.1 Organic matter removal efficiency

The Rock-Eval pyrolysis results for samples from wells NY1, N876, LY1, and LS101 before and after pretreatments were listed in Table S1. Following solvent extraction, the average values decreased from 3.40% to 2.62% for TOC, 4.07 to 0.26 mg/g for S_1, and 13.60 to 8.58 mg/g for S_2 (Fig. 2), indicating a substantial retention of soluble organic matter in shale. These soluble organic matter occupy pore space and surface sites (Li et al., 2020), potentially influencing wettability measurements. Subsequent oxidation further reduced the average values to 2.02% for TOC, 0.21 mg/g for S_1, and 5.54 mg/g for S_2 (Fig. 2), confirming the presence of organic matter connected to minerals mainly by chemical bonds that prevented their extraction (Du et al., 2022).

3.2 Changes in SSA during pretreatments

The pore wall SSA reflects the extent of organic matter coverage on pore-forming minerals, and its variation in response to different treatments indicates the removal efficiency of surface organic matter during successive reactions. The analysis of SSA changes in response to pretreatments (Table S2, Fig. 3(a)) shows that the SSA of raw samples ranged from 0.11 to 22.98 m^2/g (avg. 4.18 m^2/g). After extraction, SSA increased to 4.14-39.55 m^2/g (avg. 16.00 m^2/g), indicating that the soluble organic matter removal effectively liberated previously occupied surfaces, consistent with previous studies (DiStefano et al., 2016; Li et al., 2020). The SSA ranged from 3.68 to 39.97 m^2/g (avg. 17.49 m^2/g). Although the average SSA further increased, several samples, primarily from the deeper, higher-maturity LS101 well (R_o up to 1.2%) (Ping et al., 2017; Zou et al., 2018), showed decreased values. This may reflect the partial destruction of organic matter-hosting pores during oxidation (Li et al., 2016; Chen et al., 2017). Alternatively, water penetration into clay mineral interlayers may cause swelling and pore blockage, thereby reducing N_2 adsorption and lowering the measured surface area. In summary, sequential treatments progressively removed shale organic matter and liberate pore walls, significantly influencing the interfacial characteristics detection.

3.3 Surface roughness and surface potential characteristics

To clarify the effect of organic matter occurrence on surface potential, four lithofacies samples were selected and their pretreatment-induced surface potential changes were compared. Because contact angle and surface potential mea-

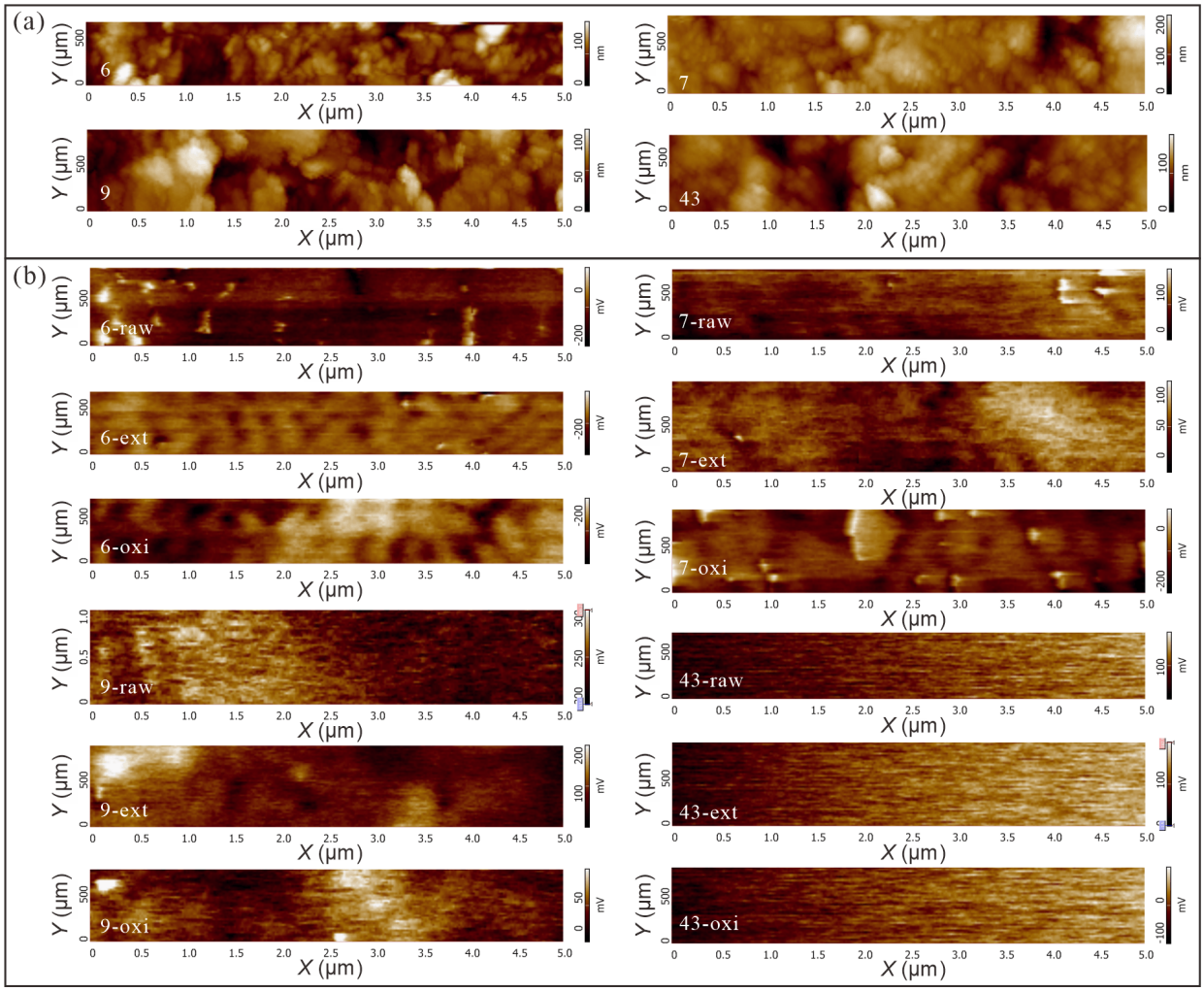


Fig. 4. (a) Surface roughness and (b) surface potential characteristics reviewed by AFM.

surements are affected by surface roughness, AFM roughness tests were first performed on pressed pellets. The surface relief was within several hundred nanometers (Fig. 4(a)), far smaller than the millimeter-scale droplet diameter used in contact angle measurements, underscoring that the pellets were suitable for both surface potential and contact angle tests. The surface potentials of shales with various lithofacies gradually shifted toward negative values after the successive treatments. However, the magnitude of change differed markedly among samples (Figs. 4(b) and 5). After extraction, the laminated mixed shale showed the largest decrease (+247.67 to +107.09 mV), the laminated calcareous shale changed little (+60.95 to +54.72 mV), the massive mixed shale decreased from -95.63 to -147.36 mV, and the layered mixed shale increased slightly from +96.24 to +101.44 mV. After oxidation, all samples shifted markedly toward negative values (Figs. 4(b) and 5): The laminated mixed shale to +36.94 mV, the laminated calcareous shale to -97.06 mV, the massive mixed shale to -248.21 mV, and the layered mixed shale to -8.54 mV. These results indicate that the surface potential and its variations are jointly controlled by mineral composition, organic matter content, and organic matter occurrence state. Solvent-extractable organic matter strongly affects laminated mixed shale, whereas organic matter is removed by oxidation, generally enhancing surface electronegativity.

3.4 Wettability response to pretreatments

Contact angles were measured before and after sequential treatments. The results showed that the contact angles of the original sample ranged from 19.12° to 96.22°, with an average of 44.64° (Fig. 3(b)). After extraction, the contact angle of shale varied within the 14.71° to 53.62° range, averaging a reduction to 30.55° (Fig. 3(b)). Following oxidation, the contact angle further decreased to the 0.00° to 42.96° range, averaging a reduction to 19.72° (Fig. 3(b)). Consequently, organic matter removal progressively shifts wettability toward hydrophilic. A few samples showed slight increases after treatment, likely due to polar organic matter adsorption and mineral composition. Polar functional groups in organic matter can enhance water-wetting (Begum et al., 2019; Jagadisan and Heidari, 2022), whereas carbonate minerals tend to be more oil-wetting under certain conditions (Sedghi et al., 2016; Taheri-Shakib et al., 2018). This reduction implies that the occurrence of organic matter will modify the surface properties significantly, pointing out the necessity of pretreatments.

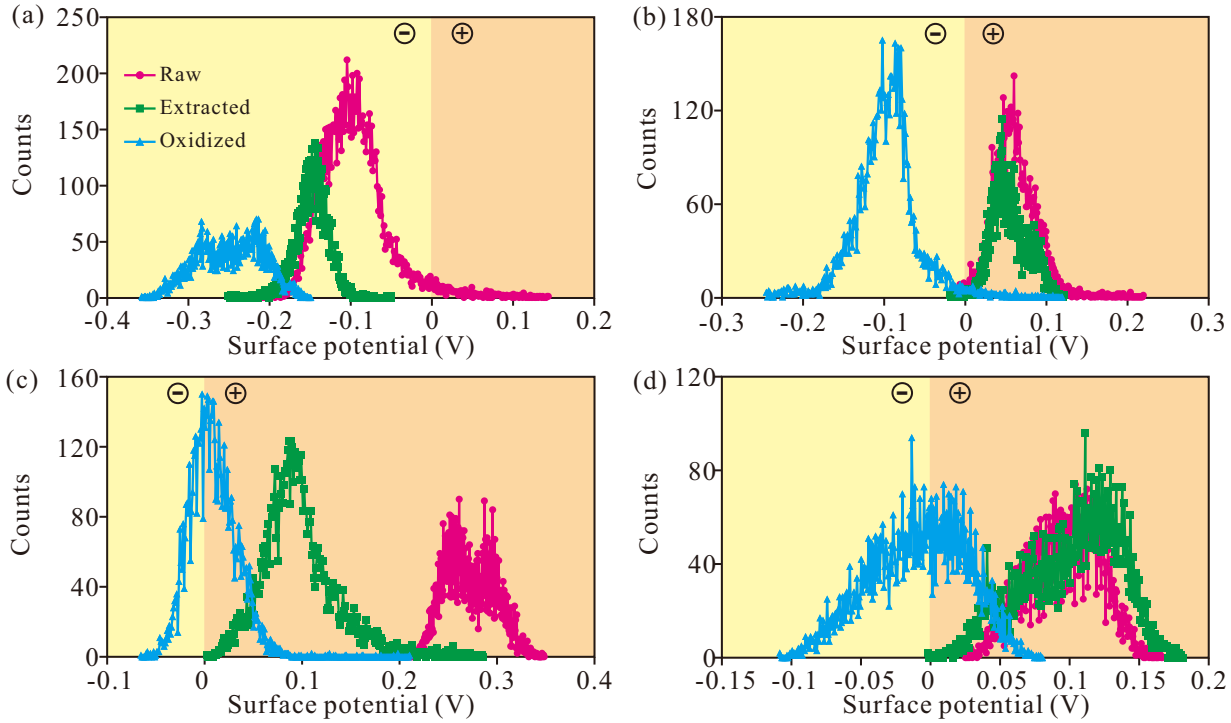


Fig. 5. Changes in surface potential in response to pretreatments: (a) Sample 6, (b) Sample 7, (c) Sample 9, and (d) Sample 43.

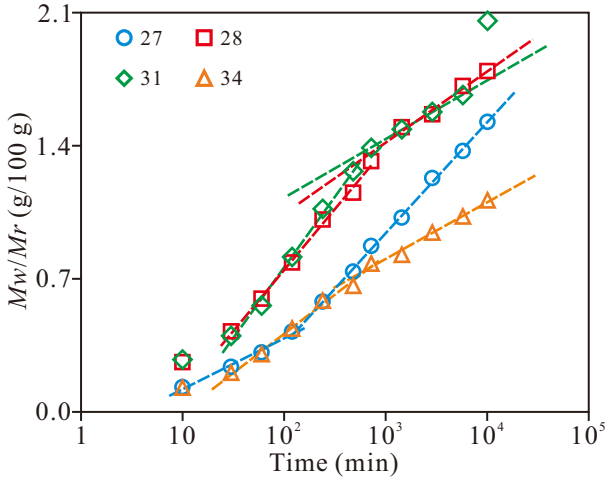


Fig. 6. Imbibed water mass versus time, where M_r represents the mass of sample and M_w denotes the mass of imbibed water at each time.

3.5 Spontaneous imbibition

All the imbibition curves exhibited a two-stage characteristic and the normalized imbibition water contents of shale samples, following the order of 31 > 28 > 27 > 34 (Fig. 6; Table S3). The slopes of the first stage of Samples 28, 31 and 34 were greater than the second stage, while Sample 27 exhibited higher slope of the second imbibition stage (Fig. 6; Table S4). The T_2 relaxation time spectra at key imbibition stages revealed distinct fluid invasion patterns (Fig. 7). Samples 27 and 34 showed limited water entry into large pores (T_2 > 2 ms), with ongoing invasion in smaller pores. Sample 27 exhibited prolonged invasion into small pores, whereas other samples (especially Samples 28 and 31) showed minimal secondary-stage invasion. This is consistent with the more pronounced increase in signal intensity in the T_2 < 2 ms range for Sample 27 during the second imbibition stage. The large pores of Samples 28 and 31 increased significantly in the final stage of imbibition (especially for Sample 31), indicating structural damage and imbibition-induced cracking (Bai et al., 2024; Mu et al., 2025). Overall, both imbibition behavior and pore-scale invasion rates varied markedly across samples.

4. Discussion

4.1 Surface characteristics modified by organic matter

4.1.1 Surface potential

According to previous analysis, the potential generally shifted gradually toward more negative values during the successive treatments (Figs. 4(b) and 5). This is because the newly exposed negative charge sites after organic matter removal are primarily contributed by silanol (Si−OH) and aluminol (Al−OH) groups (Liu et al., 2015), which are the principal active sites for acid-base chemistry on clay mineral surfaces and can form hydrogen bonds and surface complexes with polar components such as water, thereby enhancing surface hydrophilicity and electronegativity. The physical adsorption of OH^-, rather than the acidic dissociation of surface hydroxyls, may also be one of the important causes

Table 1. Comparisons of average surface potential, mineral compositions and lithofacies.

No.	Average surface potential (mV)			Clay (%)	Quartz + feldspar (%)	Carbonates (%)	Lithofacies
	Raw	Extracted	Oxidized				
6	-95.63	-147.36	-248.21	25.27	30.91	38.92	Massive mixed shale
7	+60.95	+54.72	-97.06	31.38	36.72	28.63	Laminated calcareous shale
9	+247.67	+107.09	+36.94	36.49	32.04	21.35	Laminated mixed shale
43	+96.24	+101.44	-8.54	13.1	23.82	60.27	Layered mixed shale

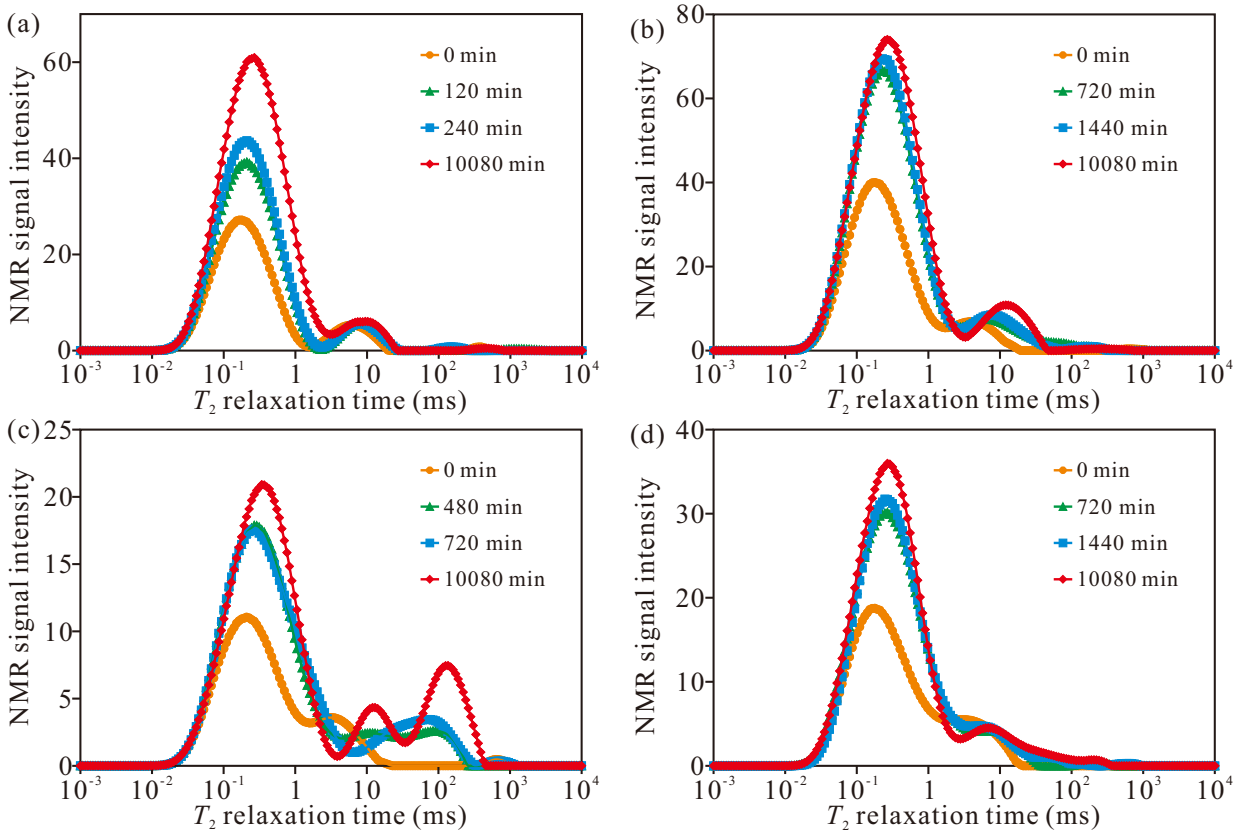


Fig. 7. Evolution of NMR transverse (T_2) relaxation time spectra during imbibition: (a) Sample 27, (b) Sample 28, (c) Sample 31, and (d) Sample 34.

of the negative shift in surface potential (Zhang et al., 2024). In contrast, organic matter-covered surfaces display a more positive surface potential owing to the masking of negative charge sites and/or the suppression of their OH^- adsorption capacity. The effects of organic coatings on the electrochemical properties of kaolinite, montmorillonite and illite have been systematically investigated. Organic coatings were found to significantly increase the negativity of surface charges, causing marked decreases in both the zero point of charge and zeta potential (Zhuang and Yu, 2002). In a Hawaiian basalt chrono sequence, it was further revealed that organic matter coatings on crystalline iron oxides and kaolinite surfaces led to flatter charging curves and lower points of zero net proton charge, demonstrating that organic coatings alter the surface electrochemical behavior of underlying minerals (Chorover et al., 2004). These results are contrary to our finding that organic matter removal leads to a negative shift in surface potential, and also differ from the common understanding that organic matter generally exhibits a negative surface potential (Kang et al., 2025). Therefore, the interfacial charge behavior of mineral-organic complexes cannot be simply inferred from either component alone, and differences in the property of surface-exposed functional groups caused by binding modes may be a more important cause of the surface potential differences.

From the perspective of occurrence state differences, solvent-extractable organic matter exerts a more pronounced effect on surface potential. After extraction, laminated mixed shale showed a decrease of ~140 mV, whereas laminated calcareous shale decreased by only ~6 mV (Table 1). This

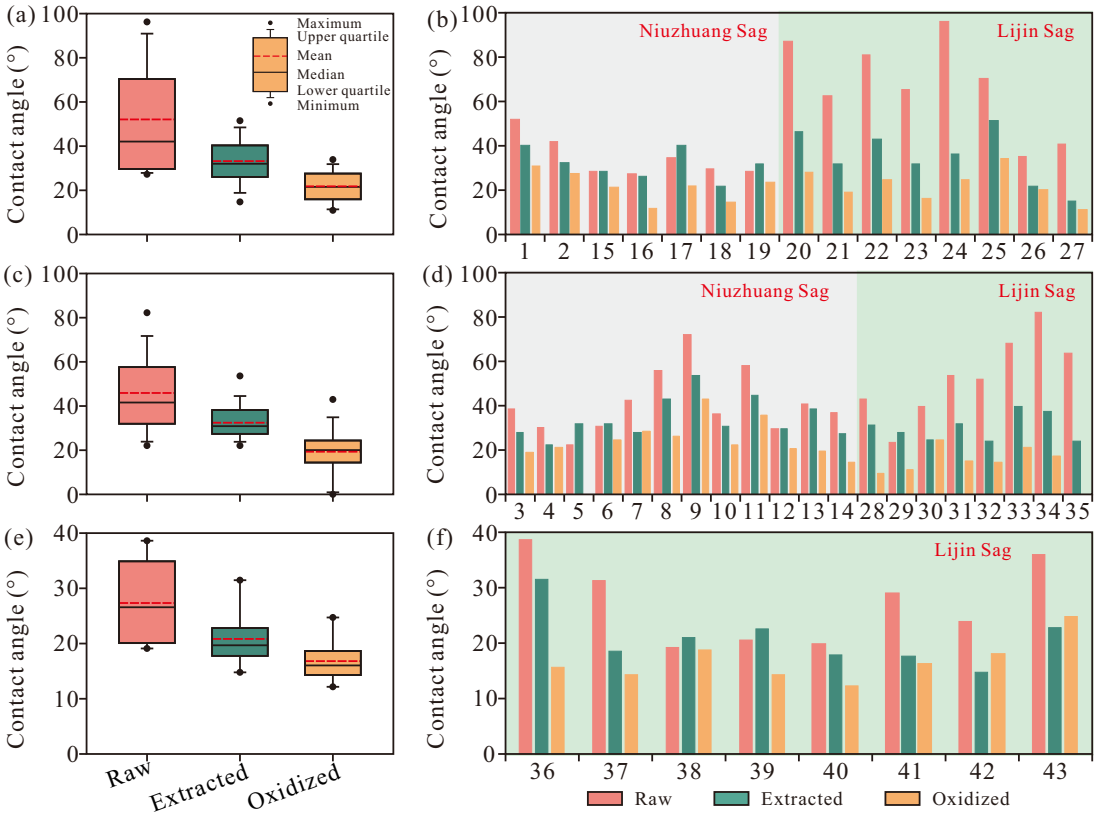


Fig. 8. Contact angle of shales from Niuzhuang Sag (gray shading) and Lijin Sag (green shading) before and after pretreatments. (a)-(b) Shales from Es_3^{lower}; (c)-(d) shales from the upper submember of Es_4^{upper}; (e)-(f) shales from the lower submember of Es_4^{upper}.

large inter-lithofacies difference reflects variations in organic matter content and occurrence mode. Massive mixed shale already had a negative surface potential (-95.63 mV), which further decreased to -147.36 mV after extraction and to -248.21 mV after oxidation (Table 1). Such changes indicate that this lithofacies has intrinsically strong negative surface charge, which is further enhanced by organic matter removal. As for laminated calcareous shale, due to its higher carbonate content being generally positively charged (Na et al., 2007), its surface potential changed minimal during extraction, and it shifted significantly toward negative values after the removal organic matter by subsequent oxidation (Table 1). These differences indicate that the controlling mechanisms of different organic matter occurrence states on pore wall electrochemical properties are lithofacies-dependent, a nuance that has not been sufficiently addressed in single-mineral studies.

4.1.2 Wettability

Molecular dynamics simulations have indicated that the water contact angle on pure kerogen surfaces is 65°-75°, while the raw sample contact angle in this study (44.64°) was lower (Wang et al., 2026a), reflecting the mixed mineral-organic character of the shale surface. As organic matter is progressively removed, the contact angle decreases from 44.64° to 30.55° after extraction and further to 19.72° after oxidation (Figs. 3(b) and 8). The final value approaches the water-wet limit expected for clean mineral surfaces. The average reductions of 14.09° and 10.82° at the two stages indicate a continuous shift toward more water-wet conditions during pretreatment. Using the Young-Dupré relation with the surface tension of water taken as 72.8 mJ/m^2, the corresponding work of adhesion increases from approximately 124.6 to 135.5 mJ/m^2 and then to 141.3 mJ/m^2 (Liu et al., 2024). The wettability and surface energy alteration are primarily governed by changes in interfacial composition and surface chemistry. Organic matter coatings reduce water wettability by masking hydrophilic mineral sites and exposing nonpolar functional groups, which lowers the surface free energy of pore walls. As soluble organic matter is removed, previously covered hydrophilic mineral sites become exposed (Fig. 3(a)), increasing surface free energy and strengthening interactions between pore walls and water. Chemically adsorbed organic matter only covers part of the mineral surface sites, and it typically contains more hydrophilic functional groups. The net change in wettability depends on the balance between residual hydrophobic organic coverage and the extent to which hydrophilic mineral surfaces have already been exposed. The progressive decrease in contact angle reflects the continuous exposure of hydrophilic mineral surfaces and the associated increase in surface energy. The contact angle and work of adhesion results consistently indicate that organic matter removal progressively shifts the surface toward a more water-wet state through the exposure of hydrophilic mineral sites and the associated increase in surface energy.

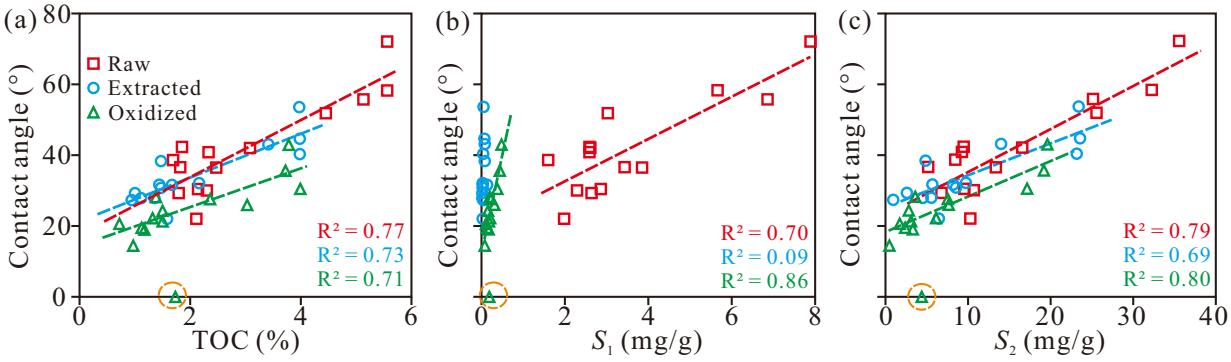


Fig. 9. Correlations of contact angle with (a) TOC, (b) S_1 and S_2 for samples before and after pretreatments.

Marked differences were observed in the contact angle changes of shale samples from different intervals and regions during sequential treatments (Fig. 8). Shales from the lower Es_3^{lower} and the upper submember of Es_4^{upper} were more responsive to treatments, with the most pronounced response in shales from the Lijin Sag. An important reason for this difference may be the thermal evolution degree of shale. Based on the relationship between burial depth and vitrinite reflectance (Zou et al., 2018), as well as the T_{max} data (Table S1), shales in the Lijin Sag and upper submember Es_4^{upper} are mainly in the peak hydrocarbon generation stage (vitrinite reflectance is approximately in the range of 0.7 to 1.0%.). These shales contain relatively high contents of soluble organic matter and respond significantly to treatments, especially to extraction. This indicates that both the occurrence states of organic matter and the transitions between these states during evolution (Du et al., 2022) significantly affect the differences in shale wettability during the successive treatment process. Further analysis of the relationship between organic matter parameters and contact angle before and after successive treatments showed that TOC, S_1 and S_2 generally exhibited good positive correlations with the rock-air-water contact angle (Fig. 9). After extraction, the pyrolysis S_1 values of the samples were very low, and the surface was essentially not covered, resulting in a poor relationship with contact angle (Fig. 9(b)). After further oxidation, organic matter decomposition released a small amount of S_1, which exhibited a strong positive correlation with contact angle (Fig. 9(b)), indicating that only a small amount of organic matter covering the pore-wall surface or remaining in pores can significantly alter interfacial wettability. More importantly, the alteration of sample wettability by organic matter is not necessarily achieved solely through covering the pore-wall surface. Although the increase in SSA after oxidation is not significant (Table S2; Fig. 2(a)), the residual organic matter after oxidation still slightly suppresses the hydrophilicity of the rock by forming mineral-organic complexes with minerals or occurring in particulate form.

Shale contains abundant organic matter in various occurrence states. The wettability and surface potential of raw shale reflect mixed contributions of bare mineral pore walls, predominantly physically organic matter coated walls, and minor chemically organic matter coated walls (Fig. 10). CH_2Cl_2 extraction exposes mineral walls previously extensively covered by solvent-extractable organic matter (Fig. 3(a)). Because clay minerals (montmorillonite, illite), the main nanopore contributors in the study area (Li et al., 2021), are more hydrophilic and negatively charged than organic matter, both hydrophilicity and negative charge were markedly enhanced. Subsequent NaClO oxidation exposed part of walls mainly covered by chemically bonded organic matter, further increasing the mineral-wall fraction and thereby further enhancing these properties. Therefore, organic matter significantly altered the interfacial properties of pore walls, transforming mineral-fluid interfacial interactions into those between mineral-organic matter complexes and fluids. The different functional groups exposed at organic matter versus mineral interfaces caused different interaction forces, strongly affecting fluid flow and occurrence. Removing organic matter in different occurrence states is thus essential for studying mineral interfacial properties.

4.2 Interfacial dynamics of fluid imbibition

Imbibition experiments establish a direct link between macroscopic surface wettability and nanoscale interfacial fluid dynamics. The positive correlation between the slope of second-stage imbibition (K_2) and contact angle demonstrates that matrix surface wettability serves as the primary control on fluid invasion into small pores (Table 2). The two-stage imbibition pattern reflects the heterogeneous nature of the confined surface. The first stage, dominated by fracture and large-pore invasion, is governed by the wettability of the most accessible surfaces. Meanwhile, the second stage, which correlates with matrix wettability, reflects the progressive invasion of fluid into smaller pores where the interfacial resistance from organic matter coatings is more significant (Yang et al., 2018). This interpretation is supported by recent work, which demonstrated that imbibition combined with NMR effectively distinguishes the wettability contributions of different pore networks, with clay-associated pores exerting a dominant control on overall imbibition behavior after organic matter extraction (Zhang et al., 2023).

T_2 relaxation time monitoring revealed a size-dependent interfacial response (Figs. 7 and 11). Fluid invasion into sub-100 nm pores was selectively hindered in samples with higher residual organic matter content (Table 2), while larger pores and fractures were less affected. This size dependence can

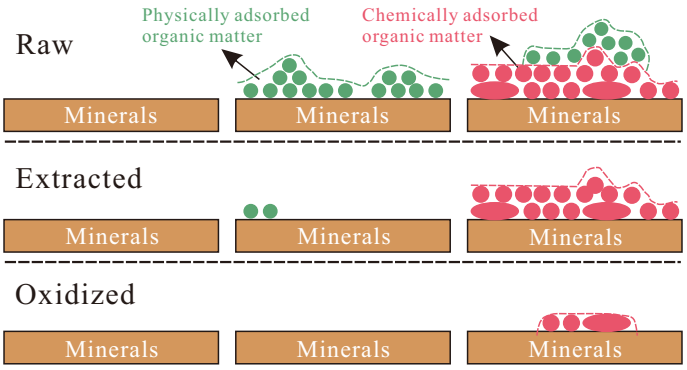


Fig. 10. Schematic diagram of pore wall conditions before and after pretreatments.

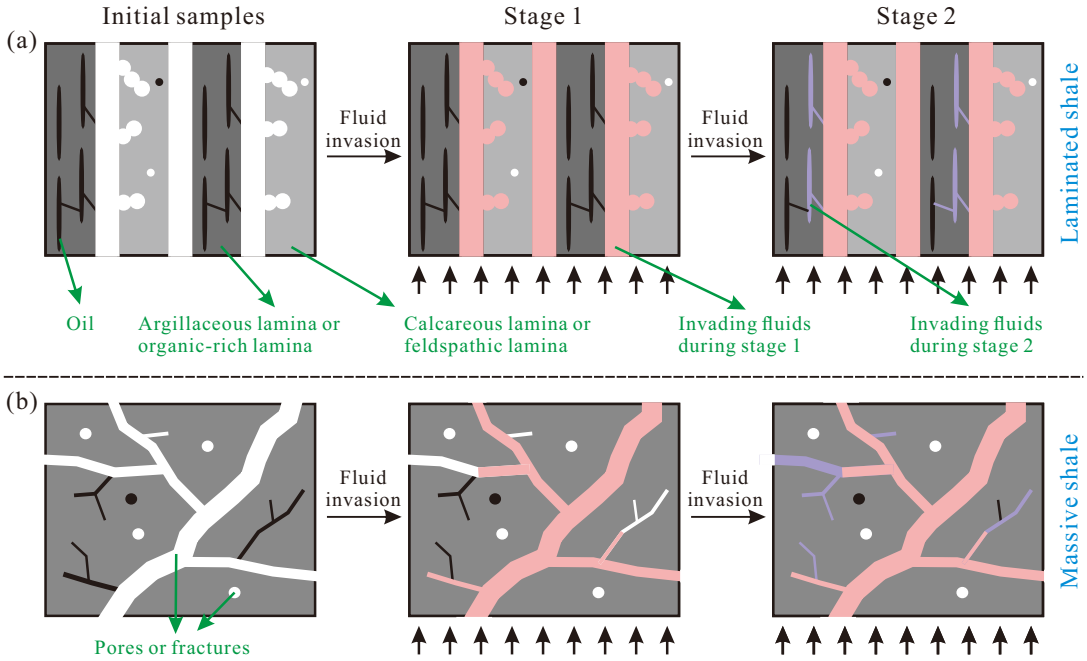


Fig. 11. Schematic comparison of (a) imbibition processes in laminated and (b) massive shale.

be understood in terms of the capillary pressure required for invasion, which scales inversely with pore radius. In small pores, the capillary pressure is high, and the presence of an organic matter coating significantly increases the interfacial resistance to water invasion. A novel technique combining NMR and vapor adsorption to decouple hydrophobic and hydrophilic pores has confirmed this scale effect. Hydrophobic nanopores mainly exist in organic matter and their nanoscale hydrophobicity is controlled by thermal maturity. Specifically, hydrophobic pores smaller than 50 nm are primarily governed by organic matter thermal maturity, while microscale pores exhibit decreased hydrophobicity due to the development of more hydrophilic clay-associated pores (Xiong et al., 2026). Molecular dynamics simulations of nanoconfined imbibition during shut-in have provided mechanistic insights into the wetting hysteresis phenomenon and the deviation of imbibition velocity from theoretical values (Jiang et al., 2024). The competitive adsorption of water molecules and oil molecules on the pore walls, along with the stratified adsorption structure of shale oil, explains the reduced imbibition efficiency in organic matter-rich nanopores. Our experimental results provide macroscopic validation of these simulation predictions, demonstrating that the primary control on fluid invasion is achieved by the reversal of interfacial wettability of small pores. This finding enables the prediction of nanoscale fluid behavior from macroscopic surface measurements, without requiring direct nanoscale observation.

By integrating lithofacies, mineralogy, TOC, contact angles, and imbibition slopes (Fig. 6; Table 2), several patterns emerge:

1) Higher TOC generally corresponds to larger contact angles (Roshan et al., 2016; Siddiqui et al., 2018), and the notably high angle in Sample 34 may be due to its high carbonate content (Al-Maamari and Buckley, 2003).
2) Smaller contact angles correlate with larger K_2, indicating that stronger hydrophilicity enhances late-stage imbibition.
3) K_1 shows poor correlation with contact angles, but aligns closely with fracture development degree.

Table 2. Comparisons of the slopes of imbibition curves, TOC, mineral compositions and lithofacies.

No.	K_1	K_2	S_1 (mg/g)	TOC (%)	Clay (%)	Quartz + feldspar (%)	Carbonates (%)	Lithofacies
27	0.1153	0.2534	2.72	1.69	25.27	30.91	38.92	Massive mixed shale
28	0.2785	0.1585	4.08	2.44	31.38	36.72	28.63	Massive mixed shale
31	0.3231	0.1332	6.76	3.68	36.49	32.04	21.35	Laminated mixed shale
34	0.1787	0.1299	6.95	3.03	13.10	23.82	60.27	Laminated calcareous shale

4) Laminated shales exhibit lower K_2 values than massive shales, likely due to the higher organic matter content (Zeng et al., 2018) and finer clay-related pores (Kuila and Prasad, 2013), which hinder water penetration into the matrix.

According to the above analyses, a schematic diagram of the shale imbibition process was proposed (Fig. 11). For laminated shales, water initially imbibes rapidly through bedding fractures and into hydrophilic mineral-associated or larger pores, corresponding to the first stage of the imbibition curve. Subsequently, imbibition progresses into organic-rich laminae or smaller pores at a considerably reduced rate, forming the second stage of the imbibition curve (Fig. 11(a)). For massive shales, water also imbibes into the rock through large pores or fractures at the initial stage, and the imbibition rate is dominated by fractures and large pores. Subsequent penetration into smaller pores follows two distinct patterns (Fig. 11(b)). The accelerated imbibition rate of Sample 27 may be attributed to its more developed small pores and lower organic matter abundance, which result in a stronger capillary force on water. In contrast, the reduced imbibition rate of Sample 28 may be due to its less developed small pores and higher organic matter abundance, which result in stronger capillary resistance to water. In summary, the imbibition process correlates closely to rock fabric, mineralogy, pore structure, fracture network, and wettability. While contact angles reflect matrix pore wettability by eliminating fracture effects, the correlation between the imbibition rate constant K_2 (massive samples) and contact angles characterizes small pore wettability. At the same time, the development degree of bedding fractures is qualitatively indicated by the initial rate constant K_1.

4.3 Implications for interfacial science and EOR

The quantitative decoupling of organic matter adsorption states on interfacial wettability advances our understanding of how organic coatings modify mineral surface properties in natural porous media. Solvent-extractable organic matter exerts a larger effect than organic matter removed by subsequent oxidation. This suggests that the molecular organization of adsorbed layers, rather than just their total amount, is a key determinant of interfacial properties (Carmody et al., 2007; Possinger et al., 2020). Solvent-extractable organic matter covers more hydrophilic mineral sites and contains more nonpolar functional groups; therefore, its removal exposes hydrophilic mineral sites and markedly alters wettability. Organic matter removed by subsequent oxidation covers only part of the mineral surface and typically contains more hydrophilic groups, so its oxidative removal produces a weaker wettability change. These results have direct implications for hydraulic fracturing design: The strong dependence of fluid invasion on mineral wettability implies that water-based fracturing efficiency depends critically on residual organic matter amount and state. In shales with high solvent-extractable organic matter content, the reduced water wettability of the interface may significantly inhibit water invasion, potentially reducing the efficiency of water-based stimulation (Xu and Dehghanpour, 2014; Singh, 2016). Active silica nanofluids can enhance shale oil recovery through synergistic wettability alteration and capillary displacement (Wang et al., 2025b); they achieve low interfacial tension and a hydrodynamic diameter of 22 nm. Micropores (< 0.07 μm) contribute 50.94% of oil recovery. Studying the wettability differences among pores of different sizes can provide an important theoretical basis for the design of wettability modification methods. Considering the variations in organic matter occurrence in shale pores of different sizes (Qi et al., 2019; Li et al., 2020), research on the relationship between organic matter occurrence and pore-wall wettability is of great significance. Nanoconfined flow in shale reservoirs exhibits slip behaviors and complex multiphase dynamics dependent on the interfacial properties (Cai et al., 2024). The experimental quantification of how organic matter adsorption states modulate surface energy and wettability offers a mechanistic basis for predicting fluid behavior in organic-rich confined spaces. The surface energy framework also has implications for CO_2 storage. CO_2 adsorption on kerogen increases the water contact angle and reduces water wettability, which is beneficial for sequestration but potentially hinders water-based EOR (Fang et al., 2024). Our successive pretreatment method characterizes baseline mineral wettability before CO_2 injection, so it would benefit the prediction of CO_2-induced alteration.

Surface potential is another critical interfacial property governing fluid-solid interactions that wettability alone cannot reveal. AFM in KPFM mode revealed that after organic matter removal, the shale surface potential shifts toward more negative values. According to the DLVO theory, electrostatic interaction between charged surfaces and fluids is a key component of disjoining pressure, directly affecting wetting and retention behavior in nanopores (Binazadeh et al., 2016). The balance between capillary pressure and disjoining pressure determines nanoscale wetting film thickness and fluid retention (Zou et al., 2021). This finding indicates that the strength of surface potential directly determines the degree of electrostatic

attraction or repulsion of fluids near the pore walls. Organic matter removal enhances the negative surface potential, which not only promotes water molecule orientation near negatively charged surfaces and leads to ordered hydration layers but also generates stronger electrostatic repulsion for negatively charged organic molecules and stronger attraction for cations. Shale wettability alteration in supercritical CO_2-brine-oil systems confirm that zeta potential changes directly indicate wettability alteration (Jiang et al., 2025). Viscoelastic surfactant fracturing fluids reduce the absolute zeta potential value and transform shale surfaces from hydrophobic to hydrophilic through charge interactions (Huang et al., 2025). These prior findings corroborate our observation that the negative shift after organic matter removal leads to water-wet conditions.

The significant change in surface potential has decisive influence on ionic surfactant selection. The adsorption of cationic surfactants is much higher than anionic surfactants on shale due to electrostatic attraction between positively charged head groups and negatively charged surfaces (Yekeen et al., 2019). Therefore, organic matter removal significantly alters the electrostatic environment of the mineral surface, which in turn controls the adsorption affinity and mobility of ionic surfactants. From an engineering perspective, traditional surfactant selection typically conducts adsorption tests on original cores. However, organic matter presence significantly changes the electrostatic environment, and the real mineral surface potential after organic matter stripping should be fully considered to avoid selection failure caused by the shielding effect. In summary, the negative shift in surface potential after organic matter removal explains the wettability shift toward water-wet conditions and reveals how electrostatic interactions control selective fluid retention and surfactant adsorption, bridging interfacial physical chemistry with engineering practice for designing more effective EOR strategies in organic-rich shale reservoirs.

5. Conclusions

This study conducts a quantitative evaluation of how different organic matter adsorption states regulate the surface characteristics and fluid invasion behavior of shale nanopores. The main conclusions are as follows:

1) Successive pretreatment enables quantitative decoupling of the surface contributions from mineral surfaces, solvent-extractable organic matter, and organic matter removed by subsequent oxidation. Both adsorption states contribute significantly to the reduced water wettability of shale surfaces, with solvent-extractable organic matter exerting a larger effect than organic matter removed by subsequent oxidation. Surface energy analysis confirms that the work of adhesion increases from 124.6 to 141.3 mJ/m^2 during organic matter removal.
2) Imbibition reveals a size-dependent interfacial response. Fluid invasion into sub-100 nm pores is selectively hindered by residual organic matter, while larger pores are less affected. The second-stage imbibition rate provides a direct proxy for the wettability of nanopores rich in residue oil. The positive correlation between the second-stage imbibition slope and contact angle establishes a quantitative link between macroscopic surface measurements and nanoscale fluid invasion behavior in confined spaces. Such a link enables the prediction of fluid behavior in organic-rich porous media without requiring direct nanoscale observation.
3) Surface electrical property and wettability are crucial for evaluating shale oil and gas exploration and development efficiency, optimizing development strategies and surfactant selection, as well as assessing CO_2-EOR performance. Residual organic matter can shield mineral surface charge and modify pore-wall wettability. Ignoring organic matter occurrence states may lead to a biased evaluation of reservoir surface properties, inappropriate surfactant selection, and unreliable prediction of CO_2-EOR performance. Integrating surface potential and wettability characterization with organic matter occurrence states is therefore essential for improving exploration and development efficiency in organic-rich shale reservoirs.
4) Shale pores of different sizes exhibit distinct wettability and fluid imbibition characteristics. To reveal how organic matter retained in matrix pores controls fluid imbibition behavior, future studies should explore imbibition experiments on shale particle samples before and after successive pretreatments.

Acknowledgments

This study was financially supported by the National Natural Science Foundation of China (Nos. 42625405 and 42302147); the Joint Funds of the National Natural Science Foundation of China (No. U24B6002) and the Open Bidding for Selecting the Best Candidates Project of Shengli Oilfield (No. 30200018-24-ZC0613-0003).

Supplementary file

https://doi.org/10.46690/ager.2026.11.02

Conflicts of interest

The authors declare no competing interest.

Open Access This article is distributed under the terms and conditions of the Creative Commons Attribution (CC BY-NC-ND) license, which permits unrestricted use, distribution, and reproduction in any medium, provided the original work is properly cited.

References

Al-Maamari, R. S. H., Buckley, J. S. Asphaltene precipitation and alteration of wetting: The potential for wettability changes during oil production. SPE Reservoir Evaluation & Engineering, 2003, 6(4): 210-214.

Bai, L., Liu, B., Huo, Y., et al. Liquid spontaneous imbibition and its time-resolved nuclear magnetic resonance within differently matured shale indications for shale pore structure and wettability. Energy & Fuels, 2024, 38(23): 22804-22819.

Begum, M., Yassin, M. R., Dehghanpour, H. Effect of kerogen maturity on organic shale wettability: A Duvernay case study. Marine and Petroleum Geology, 2019, 110: 483-

496.

Binazadeh, M., Xu, M., Zolfaghari, A., et al. Effect of electrostatic interactions on water uptake of gas shales: The interplay of solution ionic strength and electrostatic double layer. Energy & Fuels, 2016, 30(2): 992-1001.

Brunauer, S., Emmett, P. H., Teller, E. Adsorption of gases in multimolecular layers. Journal of the American Chemical Society, 1938, 60: 309-319.

Cai, J., Xia, X., Elsworth, D., et al. Evolution of multiscale pore structure and microscopic flow behavior in shales subject to fluid-rock interaction. Engineering Geology, 2026, 373: 109052.

Cai, J., Jiao, X., Wang, H., et al. Multiphase fluid-rock interactions and flow behaviors in shale nanopores: A comprehensive review. Earth-Science Reviews, 2024, 257: 104884.

Cai, J., Zhu, X., Zhang, J., et al. Heterogeneities of organic matter and its occurrence forms in mudrocks: Evidence from comparisons of palynofacies. Marine and Petroleum Geology, 2020, 111: 21-32.

Carmody, O., Frost, R., Xi, Y., et al. Adsorption of hydrocarbons on organo-clays-Implications for oil spill remediation. Journal of Colloid and Interface Science, 2007, 305(1): 17-24.

Chen, Q., Kang, Y., You, L., et al. Change in composition and pore structure of Longmaxi black shale during oxidative dissolution. International Journal of Coal Geology, 2017, 172: 95-111.

Chen, Q., Tang, X., Shi, Y., et al. Nanomechanics and pore structure evolution in organic-rich shale reservoirs during high-temperature treatment: A multi-scale analysis of microscopic stability. Advances in Geo-Energy Research, 2025, 17(3): 241-255.

Chorover, J., Amistadi, M. K., Chadwick, O. A. Surface charge evolution of mineral-organic complexes during pedogenesis in Hawaiian basalt. Geochimica et Cosmochimica Acta, 2004, 68(23): 4859-4876.

Cui, F., Meng, S., Jin, X., et al. Cross-scale analysis on shale oil initiation in nanopores: Insights into threshold pressure gradient. Advances in Geo-Energy Research, 2025, 16(2): 131-142.

DiStefano, V. H., McFarlane, J., Anovitz, L. M., et al. Extraction of organic compounds from representative shales and the effect on porosity. Journal of Natural Gas Science and Engineering, 2016, 35: 646-660.

Dong, B., Pei, Y., Mansour, N., et al. Deciphering nanoconfinement effects on molecular orientation and reaction intermediate by single molecule imaging. Nature Communications, 2019, 10(1): 4815.

Du, P., Cai, J., Liu, Q., et al. Control of different occurrence types of organic matter on hydrocarbon generation in mudstones. Petroleum Science, 2022, 19(4): 1483-1493.

Fang, H., Yue, X., Wang, L., et al. Molecular dynamics simulation of the effect of shale wettability on CO_2 enhanced oil recovery. Langmuir, 2024, 40(52): 27645-27658.

Fu, J., Xu, K., Ji, Y., et al. Water vapor sorption behavior of shale organic matter with various types and maturation. Journal of Hydrology, 2025, 663: 134223.

Huang, S., Jiang, G., Chang, Z., et al. The effect of viscoelastic surfactant fracturing fluid on methane adsorption/desorption characteristics in shale: Experimental and mechanistic study. Chemical Engineering Journal, 2025, 510: 161901.

Huang, W., Chen, B., Zhang, J., et al. Molecular evolution of organic matter humification governs ferrihydrite transformation: Interfacial electron transfer mechanisms and carbon preservation implications. Environmental Science & Technology, 2026, 60(23): 16595-16606.

Iltaf, K., Hu, Q., Fan, M., et al. Multiscale pore characterization of the New Albany Shale: Insights from complementary analytical techniques. Energy & Fuels, 2025, 39(22): 10356-10373.

Isah, A., Arif, M., Hassan, A., et al. Fluid-rock interactions and its implications on EOR: Critical analysis, experimental techniques and knowledge gaps. Energy Reports, 2022, 8: 6355-6395.

Jagadisan, A., Heidari, Z. Molecular dynamic simulation of the impact of thermal maturity and reservoir temperature on the contact angle and wettability of kerogen. Fuel, 2022, 309: 122039.

Jia, B., Yang, Y., Li, C., et al. A comprehensive review of shale wettability characterization: Mechanisms, measurements and influencing factors. Capillarity, 2025, 17(2): 38-53.

Jiang, L., Tian, L., Huang, C., et al. Experimental investigation of shale wettability and its alteration mechanisms in supercritical CO_2-brine-oil systems: Implications for CO_2 storage and enhanced oil recovery. ACS Omega, 2025, 10(19): 19840-19859.

Jiang, W., Lv, W., Jia, N., et al. Study on the effects of wettability and pressure in shale matrix nanopore imbibition during shut-in process by molecular dynamics simulations. Molecules, 2024, 29(5): 1112.

Jiao, X., He, W., Tian, Z., et al. Characterization of water micro-distribution behavior in shale nanopores: A comparison between experiment and theoretical model. Advances in Geo-Energy Research, 2024, 15(1): 79-86.

Kaiser, K., Guggenberger, G. Mineral surfaces and soil organic matter. European Journal of Soil Science, 2003, 54(2): 219-236.

Kang, Y., Ning, Z., Lyu, F., et al. Evolution of surface adhesion property and surface charge of shale organic matter at the nanoscale: Quantitative measurements by AFM and KPFM. Applied Surface Science, 2025, 695: 162919.

Kholodov, V. A., Milanovskiy, E. Y., Konstantinov, A. I., et al. Irreversible sorption of humic substances causes a decrease in wettability of clay surfaces as measured by a sessile drop contact angle method. Journal of Soils and Sediments, 2018, 18(4): 1327-1334.

Kleber, M., Bourg, I. C., Coward, E. K., et al. Dynamic interactions at the mineral-organic matter interface. Nature Reviews Earth & Environment, 2021, 2(6): 402-421.

Kok, M. V., Bal, B., Varfolomeev, M. A., et al. Thermal characteristics and model-free kinetics of oil shale samples. Journal of Thermal Analysis and Calorimetry, 2023, 148(17): 8933-8943.

Koopal, L. K. Wetting of solid surfaces: Fundamentals and charge effects. Advances in Colloid and Interface Science, 2012, 179-182: 29-42.

Kuila, U., Prasad, M. Specific surface area and pore-size distribution in clays and shales. Geophysical Prospecting, 2013, 61(2): 341-362.

Lawal, L. O., Olayiwola, T., Abdel-Azeim, S., et al. Molecular simulation of kerogen-water interaction: Theoretical insights into maturity. Journal of Molecular Liquids, 2020, 299: 112224.

Li, X., Cai, J., Gao, B., et al. Characteristics of shale pores and surfaces and their potential effects on the fluid flow from shale formation to fractures. Frontiers in Earth Science, 2021, 9: 751543.

Li, X., Cai, J., Liu, H., et al. Characterization of shale pore structure by successive pretreatments and its significance. Fuel, 2020, 269: 117412.

Li, P., Nie, H., Shen, B., et al. Wettability evaluation of hydrocarbon-bearing shales: A review of methods, controlling factors, and application. Gondwana Research, 2025, 149: 44-69.

Li, J., Zhou, S., Li, Y., et al. Effect of organic matter on pore structure of mature lacustrine organic-rich shale: A case study of the Triassic Yanchang shale, Ordos Basin, China. Fuel, 2016, 185: 421-431.

Liu, X., Cheng, J., Sprik, M., et al. Interfacial structures and acidity of edge surfaces of ferruginous smectites. Geochimica et Cosmochimica Acta, 2015, 168: 293-301.

Liu, Y., Zheng, Y., Lin, H., et al. Calculation of contact angle via Young-Dupré equation with molecular dynamic simulation: Kaolinite as an example. Colloids and Surfaces A: Physicochemical and Engineering Aspects, 2024, 697: 134469.

Lv, Q., Hou, J., Chen, T., et al. Multifactor controls on imbibition oil recovery in shale: Insights from low-field nuclear magnetic resonance. Petroleum Science, 2025, 22(12): 5128-5141.

Mayer, L. M., Schick, L. L., Hardy, K. R., et al. Organic matter in small mesopores in sediments and soils. Geochimica et Cosmochimica Acta, 2004, 68(19): 3863-3872.

Mikutta, R., Kleber, M., Kaiser, K., et al. Review: Organic matter removal from soils using hydrogen peroxide, sodium hypochlorite, and disodium peroxodisulfate. Soil Science Society of America Journal, 2005, 69(1): 120-135.

Mu, Y., Zou, C., Hu, Z., et al. Impacts of multi-scale water-rock interaction on mineral alteration, mechanical weakening and pore-fracture evolution in marine shales. Advances in Geo-Energy Research, 2025, 17(1): 68-81.

Na, C., Kendall, T. A., Martin, S. T. Surface-potential heterogeneity of reacted calcite and rhodochrosite. Environmental Science & Technology, 2007, 41(18): 6491-6497.

Pal, S., Mushtaq, M., Banat, F., et al. Review of surfactant-assisted chemical enhanced oil recovery for carbonate reservoirs: Challenges and future perspectives. Petroleum Science, 2018, 15(1): 77-102.

Ping, H., Chen, H., Jia, G. Petroleum accumulation in the deeply buried reservoirs in the northern Dongying Depression, Bohai Bay Basin, China: New insights from fluid inclusions, natural gas geochemistry, and 1-D basin modeling. Marine and Petroleum Geology, 2017, 80: 70-93.

Possinger, A. R., Zachman, M. J., Enders, A., et al. Organo-organic and organo-mineral interfaces in soil at the nanometer scale. Nature Communications, 2020, 11(1): 6103.

Qi, Y., Ju, Y., Cai, J., et al. The effects of solvent extraction on nanoporosity of marine-continental coal and mudstone. Fuel, 2019, 235: 72-84.

Roshan, H., Al-Yaseri, A. Z., Sarmadivaleh, M., et al. On wettability of shale rocks. Journal of Colloid and Interface Science, 2016, 475: 104-111.

Sedghi, M., Piri, M., Goual, L. Atomistic molecular dynamics simulations of crude oil/brine displacement in calcite mesopores. Langmuir, 2016, 32(14): 3375-3384.

Shah, K. J., Pan, S., Shukla, A. D., et al. Mechanism of organic pollutants sorption from aqueous solution by cationic tunable organoclays. Journal of Colloid and Interface Science, 2018, 529: 90-99.

Siddiqui, M. A. Q., Ali, S., Fei, H., et al. Current understanding of shale wettability: A review on contact angle measurements. Earth-Science Reviews, 2018, 181: 1-11.

Singh, H. A critical review of water uptake by shales. Journal of Natural Gas Science and Engineering, 2016, 34: 751-766.

Singh, M., Sarkar, B., Biswas, B., et al. Adsorption-desorption behavior of dissolved organic carbon by soil clay fractions of varying mineralogy. Geoderma, 2016, 280: 47-56.

Siregar, A., Kleber, M., Mikutta, R., et al. Sodium hypochlorite oxidation reduces soil organic matter concentrations without affecting inorganic soil constituents. European Journal of Soil Science, 2005, 56(4): 481-490.

Suekuni, M. T., Ezazi, M., Kwon, G., et al. Assessment of kerogen wettability from contact angle goniometry. Energy & Fuels, 2024, 38(3): 1864-1872.

Sun, M., Fu, J., Ji, Y., et al. Contrasting mechanical evolution of Bakken Shale under hydrous and anhydrous pyrolysis: A nanoindentation-based assessment. International Journal of Rock Mechanics and Mining Sciences, 2026, 203: 106526.

Taheri-Shakib, J., Rajabi-Kochi, M., Kazemzadeh, E., et al. A comprehensive study of asphaltene fractionation based on adsorption onto calcite, dolomite and sandstone. Journal of Petroleum Science and Engineering, 2018, 171: 863-878.

Wagai, R., Mayer, L. M., Kitayama, K. Extent and nature of organic coverage of soil mineral surfaces assessed by a gas sorption approach. Geoderma, 2009, 149(1): 152-160.

Walker, S. M., Marcano, M. C., Kim, S., et al. Understanding calcite wettability alteration through surface potential measurements and molecular simulations. The Journal of Physical Chemistry C, 2017, 121(50): 28017-28030.

Wang, H., Li, S., Pan, Y., et al. Study on the specific adsorption mechanism of kerogen chemical heterogeneity in shale nanopores. Fuel, 2026a, 416: 138560.

Wang, L., Liu, B., Bai, L., et al. Pore evolution modeling in natural lacustrine shale influenced by mineral composition: Implications for shale oil exploration and CO_2 storage. Advances in Geo-Energy Research, 2024, 13(3): 218-230.

Wang, R., Zhang, P., Li, J. Quantitative characterization and source tracing of fluids in shale oil and gas reservoirs: Progress and prospects. Advances in Geo-Energy Research, 2026b, 21(1): 9-12.

Wang, Z., Gao, M., Yuan, L., et al. Active nanofluids for enhanced shale oil recovery: Synergistic imbibition and multiscale pore access. Energy & Fuels, 2025b, 39(38): 18491-18502.

Xia, X., Chen, T., Wang, H., et al. Effects of salinity variations on shale imbibition behavior: Insights into the microscopic mechanisms. Petroleum Science, 2026, 23(5): 2723-2734.

Xiong, S., Yang, R., Yuan, L., et al. A novel technique to characterize hydrophobic and hydrophilic pore for shale reservoirs by nuclear magnetic resonance and vapor adsorption. Journal of Asian Earth Sciences, 2026, 305: 107067.

Xu, M., Dehghanpour, H. Advances in understanding wettability of gas shales. Energy & Fuels, 2014, 28(7): 4362-4375.

Yang, R., Hu, Q., He, S., et al. Pore structure, wettability and tracer migration in four leading shale formations in the Middle Yangtze Platform, China. Marine and Petroleum Geology, 2018, 89: 415-427.

Yekeen, N., Padmanabhan, E., Idris, A. K., et al. Surfactant adsorption behaviors onto shale from Malaysian formations: Influence of silicon dioxide nanoparticles, surfactant type, temperature, salinity and shale lithology. Journal of Petroleum Science and Engineering, 2019, 179: 841-854.

Yin, X., Gupta, V., Du, H., et al. Surface charge and wetting characteristics of layered silicate minerals. Advances in Colloid and Interface Science, 2012, 179-182: 43-50.

Zeng, X., Cai, J., Dong, Z., et al. Relationship between mineral and organic matter in shales: The case of shahejie formation, Dongying Sag, China. Minerals, 2018, 8(6): 222.

Zhang, C., Cao, J., Xiang, B., et al. Shale oil occurrence state and its controlling factors in saline lacustrine basins: Insights from sequential solvent extraction. Petroleum Science, 2025, 22(12): 4856-4874.

Zhang, M., Lv, K., Xie, M., et al. Interfacial phenomena in shale reservoirs: Molecular insights into adsorption, wettability, and nanoconfined flow. Advances in Colloid and Interface Science, 2026, 354: 103894.

Zhang, W., Yang, R., He, Z., et al. Influence of extractable organic components on shale wettability: Dongyuemiao member of Jurassic Ziliujing formation in the Fuxing area, Eastern Sichuan Basin. Marine and Petroleum Geology, 2023, 158: 106571.

Zhang, Y., Zhuang, Y., Liu, X., et al. Physical adsorption of OH- causes anomalous charging at oxide-water interfaces. Chemical Communications, 2024, 60(68): 9113-9116.

Zheng, L., Jiang, J., Xiao, W., et al. A NMR investigation of spontaneous and forced imbibition of shale under different flow and confinement conditions. Capillarity, 2025, 14(2): 53-62.

Zhu, X., Cai, J., Liu, W., et al. Occurrence of stable and mobile organic matter in the clay-sized fraction of shale: Significance for petroleum geology and carbon cycle. International Journal of Coal Geology, 2016, 160: 1-10.

Zhuang, J., Yu, G. Effects of surface coatings on electrochemical properties and contaminant sorption of clay minerals. Chemosphere, 2002, 49(6): 619-628.

Zou, A., Poudel, S., Gupta, M., et al. Disjoining pressure of water in nanochannels. Nano Letters, 2021, 21(18): 7769-7774.

Zou, Y., Sun, J., Li, Z., et al. Evaluating shale oil in the Dongying Depression, Bohai Bay Basin, China, using the oversaturation zone method. Journal of Petroleum Science and Engineering, 2018, 161: 291-301.